Paper

An Approach to Compress Information of Computer-Synthesis Hologram with Shape Adaptive Binary Tree Predictive Coding and Fast Fourier Transform Technique

Guanglin Yang* Non-member
Haiyan Xie** Non-member

A new system of Computer Synthesis Hologram (CSH) compressed and transmitted and reconstructed has been established with Shape Adaptive Binary Tree Predictive Coding (SA-BTPC) and Fast Fourier Transform (FFT) technique. In this system, the photographs can be directly calculated into the digital hologram using the holographic principle of D. Gabor. In coding, SA-BTPC algorithm adapts a non-causal, shape-adaptive predictor to decompose a digital hologram into a binary tree of prediction errors and zero blocks. Thus its coding speed is faster than JPEG baseline processing for loss compression scheme. In experiments, when its compression ratio is achieved to 0.4683% for "lossy" compression, the image lineament shape of processed CSH still can be effectively reconstructed by FFT. Moreover, the reasons have been explained why the shape adaptive predictive coding algorithm is chosen to process CSH. And the reconstructed image information of processed CSH has been compared with the reconstructed image information of original CSH. Finally, Compression ratio (R), Mean squared error (MSE) and Pear signal to noise ratio (PSNR) have been precisely calculated and analyzed to evaluate the reconstructed images variation of processed CSH. The better predictive coding model for processing digital hologram can be determined by the distortion measure.

Keywords: CSH, SA-BTPC, FFT.

1. Introduction

In Refs.(1),(2), we have explored and analyzed the pixel's amplitude and phase functions varied problems of digital Hologram transmitted in which includes the 3D information of an object, proved that the digital hologram of an object can be compressed and transmitted and reconstructed using computer image coding and optical transform techniques. But we haven't done the experiment that the digital hologram of the complexity structure image of an object is compressed and transmitted and reconstructed. Because the digital hologram of the complexity shape image is very difficult operated with computer, we have been exploring to establish a CSH compressed and transmitted and reconstructed system as shown in Fig.1. It will be able to generate conveniently the digital hologram with a computer, the photograph can be directly turned into the one, the faster coded/decoded and transmitted, and the original information of processed CSH can be reconstructed effectively in electronic system. This research will be very benefit for digital hologram developing application as a dynamical spatial filter and data storage.

In researching, we have investigated some documents for processing digital hologram. Their researching is about 3D image real-time display in the electron holographic hardware display system [3][4]. And the hardware structure complexity, cost higher, displaying the smaller size image and the digital hologram of image shape complexity is rather difficult to be made by computer operators. So the application of digital hologram has been seriously limited. In order to resolve these problems, we have adapted the holographic algorithm of D. Gabor [5], SA-BTPC [6], and FFT technique [1][2][5][7]~[9] to generate conveniently and transmit quickly and reconstruct effectively image for processing CSH with program system.

In coding, according to the information distribution shape of digital hologram is very small diffraction pattern arrays which likes one by one small hills [1][2], so we choice SA-BTPC algorithm which adapts a binary pyramid, predictive coding and Huffman coding. It is inherently progressive, and a straightforward modification of the decoder to write directly to an on-screen picture buffer allows simple, progressive, image recovery. SA-BTPC is an efficient compression method for still images and also suitable for compressing multimedia images. Its coding method includes the "lossless" or "lossy" compression for photographs and graphics. As a lossy compressor, SA-BTPC is slightly superior to JPEG for photographic images and much superior for graphics. Against a state-of-the-art lossy scheme (i.e., Said and Pearman's modified zerotree coder), it is inferior for photographs but superior for graphics and multimedia

* Image Processing Lab., Dept. of Electronics, Peking University, Beijing, 100871, China (e-mail:ygl@pku.edu.cn)
** Physics Lab. of Photo-Excited State, Graduate School of Science, Osaka City University, Osaka, 558-8585, Japan

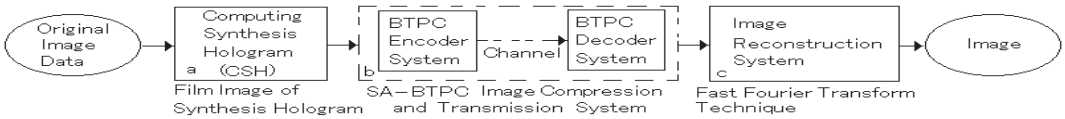

Fig. 1. A CSH compressed and transmitted and reconstructed system with SA-BTPC and FFT.

images. As a lossless compressor, SA-BTPC also has good performance on both natural images and graphics. Against a state of the art lossless scheme (i.e., Wu's CALIC), it is usually inferior for photographs and almost the same for graphics. Moreover, the coding speed of SA-BTPC is very fast [6]. In this paper, we will only discuss the "lossy" scheme to do some experiments analysis.

In reconstruction, The FFT algorithm has been adapted to process CSH. It is used to decompose a CSH into its sine and cosine components. The output of the transformation represents the image in the Fourier or frequency domain, while the input image is the spatial domain equivalent. In the Fourier domain image, each point represents a particular frequency contained in the spatial domain image information. In this paper, the Fourier Transform is used as image reconstruction and analysis [5].

In Sect.1 the system structure and the goals of processed CSH are presented. In Sect.2 the principle of CSH is described. In Sect.3 SA-BTPC algorithm model is described. In Sect.4 the image-reconstructed correlation algorithm of CSH is described. In Sects.5 and 6 the experiment analyses, discussion and the conclusion are described respectively.

2. Principle of CSH

According to theory of D. Gabor holography in on-axis reference beam, the geometry required for recording a Gabor hologram is illustrated in Ref.(5). The object is assumed to be highly transmissivity, with an amplitude transmittance

$$t(x_0, y_0) = t_0 + \Delta t(x_0, y_0) \cdots\cdots\cdots\cdots\cdots\cdots (1)$$

where t_0 is a high average level of transmittance, Δt represents the variations about this average, and $|\Delta t| \ll |t_0|$.

When such an object is coherently illuminated by the collimated source, the transmitted light consists of two components: (i) a strong, uniform plane wave passed by the term t_0, and (ii) a weak, scattered wave generated by the transmittance variations $\Delta t(x_0, y_0)$. The intensity of light incident on a photographic plate at distance z_0 from the object may be written

$$\begin{aligned} I(x,y) &= |A + a(x,y)|^2 \\ &= A^2 + |a(x,y)|^2 + Aa(x,y) + Aa^*(x,y) \\ &= A^2 + a^2(x,y) + 2Aa(x,y)cos[\psi(x,y)] \\ &\qquad\qquad \cdots\cdots\cdots\cdots\cdots\cdots (2) \end{aligned}$$

where A is the amplitude of the plane wave, $o(x,y) = a(x,y)exp[j\psi(x,y)]$ is the amplitude of the scattered light. Thus the object has, in a sense, supplied the required reference wave itself through the high average transmittance t_0. The interference of the directly transmitted light with the scattered light results in a pattern of intensity which depends on both the amplitude and the phase of the scattered wave $a(x,y)$ [5].

In terms of Eq.(2), we have made a CSH (Fig.4) from a photograph (Fig.3) using a computer, and the original image (Fig.5) of a CSH has been reconstructed by FFT.

3. SA-BTPC Algorithm

3.1 Binary Tree Structure In lossy schemes, such as DCT and wavelet pyramids shows that many quantized data attain values of zero, and blocking of zeros using run-length coding, end-of-block codewords results in good compression. In quadtree schemes, blocking of zeros can be achieved using makers within the tree to denote that all descendants of a particular node are zero. This suggests a similar strategy for the binary pyramid.

To turn the binary pyramid into a tree is to associate single-pel parents in level H_n with pairs of children in level $H_{(n-1)}$. This is done as follows:

(1) For even n, each pel in level $H(n)$ has one child $n/2$ rows above in the same column, and one child $n/2$ columns to the left in the same row.

(2) For odd n, if a pel's parent is below it, then its children are $(n-1)/2$ rows below it and $(n-1)/2$ columns to its left and right.

(3) For odd n, if a pel's parent is to its right, then its children are $(n-1)/2$ rows below it, one is $(n-1)/2$ columns to its right, and the other is $3(n-1)/2$ columns to its right.

This ordering scheme ensures that a pel's descendants form a square or a $2:1$ rectangle. A branch-termination or leaf codeword for a particular pel indicates that all its descendants are zero.

To confirm that the binary tree representation makes for efficient representation of blocks of zeros, test images are coded with and without branch termination codewords. In addition, run-length coding of strings of zeros was implemented and tested. In each case, the tree representation with branch termination codewords provided most efficient coding [6] as shown in Fig.2 (a).

3.2 Fixed Prediction Coding In conventional predictive coding, the design goal of the binary tree predictor is to minimize prediction error variance. Every new pel to be predicted is at the center of a square of four equidistant pels from earlier levels or bands. Fig.2 (b) illustrates the case where X is in the current level and is surrounded by A, B, C and D from earlier levels. U and V are earlier pels in the current band. Some previous researchers have simply used the bilinear prediction $X' = (A+B+C+D)/4$, while others have tried nonlinear schemes to select a subset of the four corner.

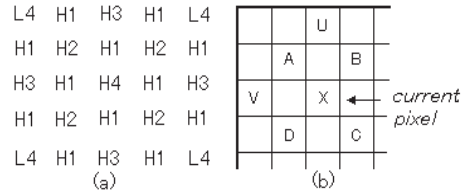

Fig. 2. (a) The image pels showing membership in the finest four bands of the binary pyramid; (b) Predictor coding template of SA-BTPC, Pel X in the current band and its four predictors A, B, C, and D. U and V are earlier pels in the current band.

This section will explain why a nonlinear approach that selects a pair of opposite corners (i.e., either $X' = (A + C)/2$ or $X' = (B + D)/2$) is effective. In processing CSH, the pixel diffraction information distribution of Hologram includes along most edges, the gradient changes direction slowly. Assuming that within an ABCD square, the gradient direction (but not its magnitude) is constant, one of the two diagonals AC, BD is closer to the gradient direction than the other. The case of a luminance edge is at an arbitrary orientation to the pel grid, and in this case the diagonal AC is closer to the gradient direction, so BD is in the direction of lesser surface slope. If the central point and its four neighbors are projected onto the plane defined by the gradient, then they have the arrangement.

The opposite pels in the direction of least surface slope (in this case B and D) are always closest to the central point in this projection. As long as the ABCD square straddles, only a single edge or line, the two opposite pels closest to X in this projection are also always closest in value to X. Furthermore, when there is no second derivative sign change in the ABCD square, the average of the two closest opposite pels is sure to be a better linear estimate of the value at X than the average of the other two pels (and therefore of the 4-pel bilinear average). At a second derivative sign change, the shape of the edge between the surround pels in their projection onto the gradient determines the best linear average. In most cases, the foot of the edge will be blurred in the same way as the shoulder of the edge, and the closest-opposite-pels average will be at least as good as any other average.

How can the pair of opposite pels closest to X in the gradient-direction projection be identified ? If the gradient magnitude is of the same sign throughout the ABCD square, that is, if the square is on a smoothly-shaded surface or straddling an edge, the two opposite pels closest to X on the line of the gradient are closer in value to each other than are the pels of the other diagonal. Furthermore, these two pels have the middle two values of the four predictors. However, in this case, if the ABCD square straddles a line, then the two pels closest to X on the gradient direction projection, although still closest to X in value, are not necessarily closer in value to each other than the pels of the other diagonal. For example, shows a contrary case, the situation of straddling a line can be detected because the highest and lowest values are attained by adjacent pels in the predictor square.

To summarize, if the four surround pels come from a smoothly shaded area of the image or straddle a single edge where the gradient direction changes very little, the pair of opposite corner pels closest in value to each other are the pair closest to the center point in a projection onto the gradient, and their average is the best estimate of the value at the center. The simplest, fast, fixed predictor is the closest-opposite-pair predictor, which always uses this average. In experiments, closest-opposite-pair prediction has proven superior to other approaches, including median prediction. However, as discussed above, its effectiveness depends on the local surface shape, that is, the ordering of the four corner prediction pels. This leads to the idea of an adaptive prediction strategy, based on shape [6].

3.3 Shape Adaptive Prediction Coding The closest-opposite-pair predictor performs well on smooth shading and edges. To design a shape-adaptive predictor, it is necessary to consider the other types of local surface shape that might be encountered, and to test appropriate alternative strategies. For example, consider graphics boundaries, which typically line up horizontally or vertically. For a horizontal boundary, predictor pels A and B have one value and pels C and D a different value. The closest-opposite-pair predictor estimates the center pel X as the average of these, but its true value is either one or the other. Moreover, the correct value will probably have been attained by the previous pel in the same band, pel V, in Fig.2 (b). In the same way, if A and D are equal, and B and C are equal but different to A and D, then U is likely to be the best predictor. A similar argument can be made for the case where $(A = C \neq B = D)$. Indeed, lines (ridges and valleys) are in general poorly represented by the closest-opposite-pair predictor, and experiments show that in many cases it is worth spending one bit to indicate which of the two opposite pairs is to be used as predictor.

How shape considerations are applied in designed the adaptive BTPC predictor. This is a key problem. The 14 possible shapes of the Prediction Square have been listed in Ref.(6), in terms of the order of amplitudes of the four corner pels. These shapes can appear in any orientation. The table of Ref.(6) gives comments on the performance of the closest opposite pair predictor and shows if and how it can be improved for each shape. The adaptive BTPC predictor applies the shape rules shown in Ref.(6) to achieve a more accurate estimate of the center pel value. To achieve high speed, at the cost of a slight decrease in compression performance, BTPC converts to a fixed predictor in low activity, smoothly shaded areas [6].

4. Image Reconstructed Algorithm of CSH

4.1 Correlation Technique According to Huygens Fresnel principle [7], the formula for diffraction is

$$\psi(\acute{x}, \acute{y}, \acute{z}) = \int_{y_{min}}^{y_{max}} \int_{x_{min}}^{x_{max}} h(x, y)$$

$$\cdot \frac{A\exp[jk\sqrt{(\acute{x}-x)^2+(\acute{y}-y)^2+\acute{z}^2}]}{\sqrt{(\acute{x}-x)^2+(\acute{y}-y)^2+\acute{z}^2}}dxdy \quad \cdots\cdots\cdots\cdots\cdots\cdots (3)$$

where $h(x,y)$ is the transmission of the digital hologram. In the present application, the following far field approximation can be used.

$$\psi(\acute{x},\acute{y},\acute{z}) = \frac{A\exp[\frac{j2\pi\acute{a}}{\lambda}]}{\acute{z}} \int_{y_{min}}^{y_{max}} \int_{x_{min}}^{x_{max}} h(x,y) \cdot \exp[\frac{i\pi}{\lambda\acute{a}}((\acute{x}-x)^2+(\acute{y}-y)^2)]dxdy \quad \cdots\cdots\cdots\cdots\cdots\cdots (4)$$

This is the Rayleigh-Sommerfeld equation and is of the form

$$\psi(\acute{x},\acute{y},\acute{z}) = B(\acute{z}) \int_{y_{min}}^{y_{max}} \int_{x_{min}}^{x_{max}} h(x,y) \cdot P(\acute{x}-x,\acute{y}-y,\acute{z})dxdy; \cdots\cdots\cdots (5)$$

$$B(\acute{z}) = \frac{A\exp[\frac{j2\pi\acute{a}}{\lambda}]}{\acute{z}}; P(\acute{x},\acute{y},\acute{z}) = \exp[\frac{i\pi}{\lambda\acute{a}}(\acute{x}^2+\acute{y}^2)].$$

Therefore, simulated diffraction can be approximated as a convolution between the hologram $h(x,y)$ and a complex pattern $P(x,y,\acute{z})$ which depends on the distance from the hologram $\acute{z}$. All the terms including $(\acute{x}-x)$ and $(\acute{y}-y)$ are squared, so using $(x-\acute{x})$ and $(y-\acute{y})$ instead would have no effect. From Eq.(5) to analyze, $h(x,y)$ and $P(x,y,\acute{z})$ are a correlation. For each value of $\acute{z}$, $P(x,y,\acute{z})$ is not dependent on x and y, it is shift-invariant. From the correlation theorem [7]~[9], therefore we can get

$$\psi(\acute{x},\acute{y},\acute{z}) = F^{-1}[F[h]F[P]] \cdots\cdots\cdots\cdots\cdots\cdots (6)$$

where F denotes a 2D Fourier transform and F^{-1} an inverse Fourier transform. Using correlation to reconstruct the image therefore needs three times 2DFFT.

4.2 Fourier Transform Technique According to equation (5), we can obtain

$$\psi(\acute{x},\acute{y},\acute{z}) = \frac{A}{\acute{z}}\exp[\frac{j2\pi\acute{a}}{\lambda}]\exp[\frac{j\pi(\acute{x}^2+\acute{y}^2)}{\lambda\acute{a}}] \cdot \int_{y_{min}}^{y_{max}} \int_{x_{min}}^{x_{max}} h(x,y)\exp[\frac{j\pi(x^2+y^2)}{\lambda\acute{a}}] \cdot \exp[\frac{j2\pi(\acute{x}x+\acute{y}y)}{\lambda\acute{a}}]dxdy \cdots\cdots\cdots (7)$$

If we then set $u = \frac{\acute{x}}{\lambda\acute{z}}$ and $v = \frac{\acute{y}}{\lambda\acute{z}}$, we can get

$$\psi(u,v,\acute{z}) = D(u,v,\acute{z}) \cdot \int_{y_{min}}^{y_{max}} \int_{x_{min}}^{x_{max}} T(x,y,\acute{z}) \cdot \exp[j2\pi(ux+vy)]dxdy \cdots\cdots\cdots (8)$$

$$D(u,v,\acute{z}) = \frac{A}{\acute{z}}\exp[\frac{j2\pi\acute{a}}{\lambda}]\exp[j\pi\lambda\acute{z}(u^2+v^2)]; and$$

$$T(\acute{x},\acute{y},\acute{z}) = h(x,y)\exp[\frac{j\pi(x^2+y^2)}{\lambda\acute{a}}].$$

This means that the image can be reconstructed using just one Fourier transform.

4.3 Reconstruction with Fourier Transform Technique According to Ref.(7),~ (9), we can perform FFT. One routine computes the 2D Discrete Fourier Transform of a sequence of hologram data h_{i_d,j_d}. Its transform H_{i_d,j_d} is defined by

$$H_{i_\delta,j_\delta} = F[h] = \frac{1}{\sqrt{n_x n_y}} \sum_{j_d=0}^{n_y-1} \sum_{i_d=0}^{n_x-1} h_{i_d,j_d} \cdot \exp[-j2\pi(\frac{i_d i_\delta}{n_x} + \frac{j_d j_\delta}{n_y})] \cdots\cdots\cdots (9)$$

where $i_d, i_\delta = 0,1,...,n_x-1$, $j_d, j_\delta = 0,1,...,n_y-1$. The hologram data values are real so the inverse Fourier transform of $h_{i_d,j_d}F^{-1}[h]$ would be the complex conjugate of H_{i_d,j_d}. The formula for reconstruction using one $2DFFT$ was given by equation (8), with $x_{min} = -(\frac{n_x}{2})\Delta$, $x_{max} = (\frac{n_x}{2}-1)\Delta$, $y_{min} = -(\frac{n_y}{2})\Delta$ and $y_{max} = (\frac{n_y}{2}-1)\Delta$ to write equation (8) written in discrete form using equation $\lambda\acute{z} = r_1^2(\frac{z+b}{z})^2 = r_{1z}^2$, we get

$$\psi_{i_\delta,j_\delta} = D_{i_d,j_d} \sum_{-\frac{n_y}{2}}^{\frac{n_y}{2}-1} \sum_{-\frac{n_x}{2}}^{\frac{n_x}{2}-1} T_{i_d,j_d} \cdot \exp[j2\pi(i_d i_\delta + j_d j_\delta)\Delta^2\alpha(\frac{a}{r_1(a+b)})^2] \cdots\cdots\cdots\cdots\cdots (10)$$

$$D_{i_d,j_d} = \frac{A}{z+b}\exp[j2\pi\frac{(a+b)}{\lambda}] \cdot \exp[j\pi\frac{a^2((\Delta\alpha i_d)^2+(\Delta\alpha j_d)^2)}{r_1^2(a+b)^2}]; and$$

$$T_{i_d,j_d} = h_{i_d,j_d}\exp[j\pi\frac{a^2((\Delta\alpha i_d)^2+(\Delta\alpha j_d)^2)}{r_1^2(a+b)^2}]$$

If the equation (10) is to be used, the limits of the summations need to be altered. If we use the substitution $k_d = i_d + \frac{n_x}{2}$ and $l_d = j_d + \frac{n_y}{2}$, we can rewrite equation (11) as

$$\begin{aligned}\psi_{i_\delta,j_\delta} &= D_{i_\delta,j_\delta} \sum_{0}^{n_y-1} \sum_{0}^{n_x-1} T_{k_d-\frac{n_x}{2},l_d-\frac{n_y}{2}} \cdot \exp[j2\pi((k_d-\frac{n_x}{2})i_d + (l_d-\frac{n_y}{2})j_d) \cdot \Delta^2\alpha(\frac{a}{r_1(a+b)})^2] \\ &= D_{i_\delta,j_\delta}\exp[-j\pi(i_d n_x + l_d n_y) \cdot \Delta^2\alpha(\frac{a}{r_1(a+b)})^2] \sum_{0}^{n_y-1} \sum_{0}^{n_x-1} T_{k_d-\frac{n_x}{2},l_d-\frac{n_y}{2}} \cdot \exp[j2\pi(\frac{k_d i_d}{n_x})n_x\Delta^2\alpha(\frac{a}{r_1(a+b)})^2] \cdot \exp[j2\pi(\frac{l_d j_d}{n_y})n_y\Delta^2\alpha(\frac{a}{r_1(a+b)})^2] \end{aligned} \cdots\cdots\cdots\cdots\cdots (11)$$

The scaling property of the 2D Fourier transform[10] is given by

$$h_{\delta_x i_d,\delta_y j_d} \Longleftrightarrow \frac{1}{|\delta_x\delta_y|}H_{\frac{i_d}{\delta_x},\frac{j_d}{\delta_y}} \cdots\cdots\cdots\cdots (12)$$

therefore, we have

$$\psi_{\frac{i_d}{\delta_x},\frac{j_d}{\delta_y}} = D_{\frac{i_d n_x}{\delta_x},\frac{j_d n_y}{\delta_y}} \exp[-j\pi(\frac{i_d}{\delta_x}+\frac{j_d}{\delta_y})] \cdot \Delta^2\alpha(\frac{a}{r_1(a+b)})^2\frac{\sqrt{n_x n_y}}{|\delta_x\delta_y|} \cdot F^{-1}[T_{(k_d-\frac{n_x}{2})\delta_x,(l_d-\frac{n_y}{2})\delta_y}] \cdots\cdots\cdots (13)$$

$$\delta_x = \Delta^2\alpha(\frac{z}{r_1(z+b)})^2 n_x; \delta_y = \Delta^2\alpha(\frac{z}{r_1(z+b)})^2 n_y.$$

The pixels in the reconstructed image represent an area $\frac{1}{\delta_x} \times \frac{1}{\delta_y}$ times the detector pixel size. For the single Fourier transform technique, we therefore have

$$\frac{P_{sr}}{P_{sh}} = \begin{cases} (\frac{r_1(z+b)}{z\Delta})^2\frac{1}{n_x}(\frac{b}{z}) & \text{in the } x \text{ direction;} \\ (\frac{r_1(z+b)}{z\Delta})^2\frac{1}{n_y}(\frac{b}{z}) & \text{in the } y \text{ direction.} \end{cases}$$

The size of the pixels in an image reconstructed by correlation, however, depends only upon the relative displacements of a point source and the center of its shadow for any z.

$$\frac{P_{sr}}{P_{sh}} = \frac{z}{b} \text{in both } x \text{ and } y \text{ directions.} \cdots\cdots\cdots (14)$$

where P_{sr} is Pixel size reconstructed image plane; P_{sh} is Pixel size synthesis hologram. If correlation is used, the sizes of the pixels in the image have a straightforward relationship to the hologram pixel size. This relationship depends only upon z and b. If only one Fourier transform is used, the first zone radius of the zone plate,r_1 , detector pixel size, Δ and the number of pixels in the x and y directions, n_x and n_y also have an effect. In this case, the reconstructed image can be a very different size than one would intuitively expect. Its detail can be seen in Ref.(5), (7) $\sim$ (10).

5. Experimental Analyses and Discussion

5.1 Compression Ratio and Distortion Measure The observation by the eye, and comparing the original with the processed CSH, but it is not enough to determine objectively the quality and information distribution of the image. Therefore, we must adapt the concept of MSE and $PSNR$.

According to the image processing theories, the evaluating function (i.e., Eqs. (15), (16), (17)) of the compression efficiency and the distortion measure can be written [11]. In this system, R, MSR and $PSNR$ of the processing CSH can be precisely calculated as shown in Table 1 and Fig.9.

$$R = \frac{S_c}{S_o} \cdots\cdots\cdots (15)$$

Where R is the compression efficiency, S_o is defined as the size of the original image data and S_c is the size of the compressed image data.

$$MSE = \frac{1}{512^2}\sum_{x=1}^{x=512}\sum_{y=1}^{y=512}[f(x,y)-\bar{f}(x,y)]^2 \cdots\cdots\cdots (16)$$

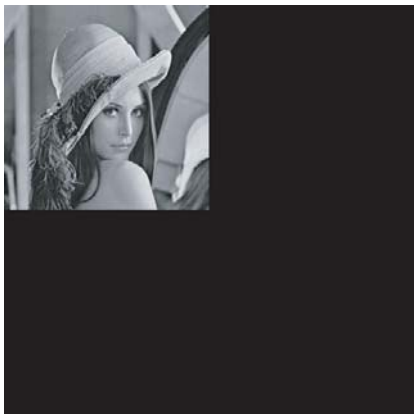

Fig. 3. Original image (size: $7.11 \times 7.11 inch^2$, $512 \times 512 pixel^2$, 257kb, $8bpp/256$.).

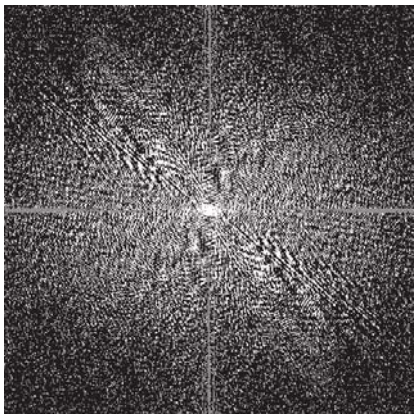

Fig. 4. A film image of computer synthesis hologram (size:$7.11 \times 7.11 inch^2$, $512 \times 512 pixel^2$, 257kb, $8bpp/256$.).

Fig. 5. A reconstructed image of CSH using FFT (size:$7.11 \times 7.11 inch^2$, $512 \times 512 pixel^2$, 257kb, $8bpp/256$.).

$$\text{PSNR} = 10\log_{10}\Big[\frac{x_p^2}{\text{MSE}}\Big](\text{dB}) \cdots\cdots\cdots (17)$$

where x, y are $1 \sim 512$. $f(x,y)$ is CSH's image function, $\bar{f}(x,y)$ is the processed CSH's image function, x_p is the peak to peak value 255 of the image data. In Table 1, relationship data about $R(\%)$, MSE and PSNR of reconstructed images of processed CSH are described. $q(N)$ is

Fig. 6. A image of compressed CSH using SA-BTPC encoding (size:7.11×7.11$inch^2$, 512×512$pixel^2$, 2kb, 8bpp/256, q(N)=20, $R = 1.0673\%$.).

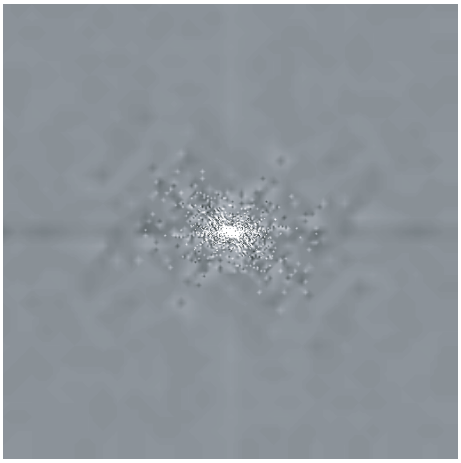

Fig. 7. A image of decompressed CSH using SA-BTPC decoding (size:7.11 × 7.11$inch^2$, 512 × 512$pixel^2$, 257kb, 8bpp/256, q(N)=20.).

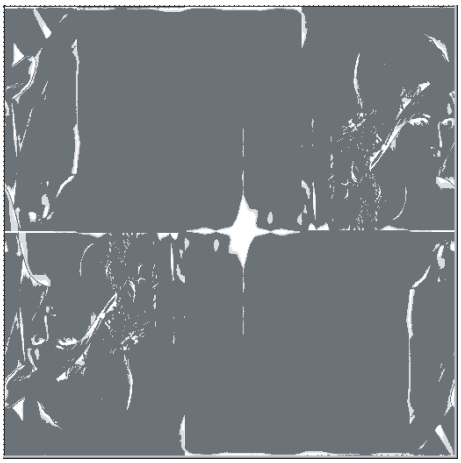

Fig. 8. A reconstructed image of decompressed CSH using FFT (size: 7.11×7.11$inch^2$, 512×512$pixel^2$, 257kb, 8bpp/256, q(N)=20.).

defined as the quatization parameter. PSNR is the peak signal noise ratio of reconstructed images of processed CSHs.

Through analyzing Fig.9, the more precision relationship of this system can be found about R, MSE and PSNR of CSH compressed and transmitted and reconstructed. In terms of these data, the "lossy" compression algorithm model can be determined. To analyze Table 1 and Fig.9, we can understand the relation, i.e., $R(\%)$ is inversely proportional to MSE and directly proportional to PSNR.

5.2 CSH Transmitted Error and Reconstructed Image Quality In system experiments, a photograph (Fig.3) is transformed into a CSH (Fig.4), and encoded as Fig.6 using SA-BTPC and then Fig.6 is transmitted and decoded as Fig.7. And the image (Fig.8) is reconstructed from Fig.7 by FFT. Finally, the evaluating functions of distortion measure of processing CSH are adapted to determine the reconstructed image quality of original CSH and the processed CSH. Using program, we have calculated the relative parameters and curves of MSE, PNSR and $R\%$ as shown in Fig.9 and Table 1, so we can analyze and get some experiment results.

In coding experiment, because a shape-adaptive predictive coding with a binary tree structure is applied, its coding speed is higher. From reconstructed images (i.e., Figs.5, 8) to analyze, its calculating error is smaller, the noise of reconstructed images is lesser except that the center part noise is due to the assumptive conditions.

In reconstructing experiment, the images (Figs.5, 8) can been clearly reconstructed from CSH and processed CSH (Figs.4, 7) using FFT, but the central part of reconstructed-image exists a certain noise, and it is the twin image. The reason is that the assumptive conditions of D. Gabor holography have some limitation.

In distortion measure, when the $q(N)$ value is increased generally, the MSE value are generally decreased, however, the $R\%$ and PSNR is generally in-

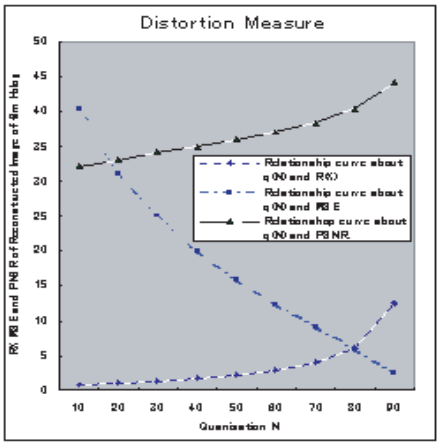

Fig. 9. Relationship curves about MSE, $PNSR$ and $R\%$ of reconstructed images of processed CSH.

Table 1. Relationship data about $R\%$, MSE and PSNR of reconstructed images of processed CSH.

$q(N)$	5	10	20	30	40
$R(\%)$	0.4683	0.7584	1.0673	1.3143	1.7061
MSE	45.4823	40.3765	30.0073	25.3511	20.6890
$PSNR$	31.8753	32.0695	33.3585	34.0908	34.9734
$q(N)$	50	60	70	80	90
$R(\%)$	2.2285	2.8121	3.9327	6.1129	12.5524
MSE	15.8310	12.8905	9.4183	6.0016	2.5740
$PSNR$	36.1357	37.0281	38.3911	40.3482	44.0248

creased as shown in Fig.9 and Table 1. The reconstructed image quality of processed CSH generally become better. Consequently, according to the parameters of curves, we can choose a better transmission model.

As comparing Fig.5 with Fig.8, we have found some problems, i.e., reconstructed twin images, and there are some noises in center part. The reasons of causing these problems are that Gabor hologram algorithm has some limitations in practice [5]. Perhaps the most serious limitation is inherent in the assumption $|\Delta t| \ll |t_0|$ of a highly transparent object, and the consequent assumption $a(x, y) \ll A$ that followed. In fact, if the object is of low average transmittance, this particular wave component may be the largest transmitted term, as a consequence, may entirely obliterate the weaker images. This restriction seriously hampers the applications of Gabor holograms. The other serious limitation lies in the generation of twin images, rather than one image [5]. In order to resolve these problems, we are exploring other holographic algorithm.

6. Conclusion

A CSH compressed and transmitted and reconstructed system has been established with SA-BTPC and FFT technique. In this system, the general photograph can be directly calculated into the digital hologram. This digital hologram can be more quickly shape adaptive predictive coded using SA-BTPC, whose calculating precision is better, and the complexity shape image can be effectively reconstructed after shape adaptive predictive coded and decoded, thus the system's calculating speed is faster than JPEG baseline processing for loss compression. The potential applications of this system include the complex facsimile equipment for digital hologram input and recording [12]. The future, perhaps it may be applied in the coding techniques for holographic data storage systems [13]. This processing method has the potential application promising.

(Manuscript received April 14, 2003,
revised Sep. 17, 2004)

References

(1) G. Yang and E. Shimizu: "CGH Compression and Transmission and Reconstruction of CGH with JPEG Baseline Processing and Fresnel Transforming Technique", *IEEJ Trans. EIS*, Vol.121-C, No.8, pp.1326-1333 (2001-8)
(2) G. Yang, E. Shimizu: "Information Compressed and Transmitted and Reconstructed System of CGH with LOCO-I Image Processing and Fraunhofer Transforming Technique", *IEEJ Trans. EIS*, Vol.120-C, No.11, pp.1520-1527 (2000-11)
(3) H. Yoshikawa and E. Tanji: "Method of Holographic 3-D Image Compression with a Standard Coding", *The Journal of the ITE of Japan*, Vol.47, No.12, pp.1678-1680 (1993-12)
(4) L. Mark: "Holographic bandwidth compression using spatial subsampling", *Optical Engineering*, Vol.35, No.6, pp.1529-1537 (1996-6)
(5) J.W. Goodman: Introduction to Fourier Optics, Copyright © 1968 by McGraw-Hill, Inc, New York (1968)
(6) J.A.Robinson: "Efficient general-purpose image compression with binary tree predictive coding", IEEE Trans. *Image Proc.*, Vol.6, No.4, pp.601-607 (1997-4)
(7) I.K. Woodgate: "Zone Plate Encoded Holography in the Optical Region", Ph. D. thesis, School of Physics and Space Research, University of Birmingham (1996-6)
(8) Numerical Algorithms Group Limited, Oxford, UK. The NAG Fortran Library Manual, Mark 14 (1990)
(9) C.E. Unwin and T.D.Beynon: "Reconstruction of Images from Gabor Zone Plate Gamma Ray Holography", Ph. D. Mid-term Research Report in University of Birmingham (1997-9)
(10) A.K. Jain: "Fundamentals of Digital Image Processing", Prentice-Hall International, Inc, University of California, Davis (1989)
(11) W.D. Kou: Digital Image Compression Algorithms and Standards, Copyright © 1995 by Kluwer Academic Publishers, Boston/Dordrecht/London, pp.149-150
(12) V.V. Komar: "Progress on the Holographic Movie Process", in the USSR, in SPIE, Bd. 120, S. 127-144 (1977)
(13) J.J. Ashley, M. Blaum, and B.H. Marcus: "Report on Coding Techniques for Holographic Storage", IBM Research Report, Published in RJ10013 (1996)

Guanglin Yang (Non-member) is an Associate Prof. in School of Electronics Engineering & Computer Science, Peking University from Aug. 2002. He received his Dr. Eng. degree from School of Engineering, Osaka City University of Japan in Sept. 2001 and his M. Eng. degree from Dept. of Opto-electronics Engineering, Huazhong University of Science & Technology of China in June 1993. He became a lecturer in Faculty of Automatic Control Engineering, Beijing University of Aeronautics and Astronautics of China in Sept. 1994. His research interests mainly include the optical information processing, image processing, artificial neural network, intelligent infrared detecting, and digital control technique. He respectively is a member of IEEE and CIE.

Haiyan Xie (Non-member) is pursuing Ph. D. degree in School of Science, Osaka City University of Japan from April 1999. She received her M. S. degree from School of Science, Osaka City University of Japan in March 2002. Moreover, she received her B. and M. Eng. degrees from Dept. of Opto-electronic & Scientific Instrumentation Engineering, Zhejiang University of China in July 1990 and Dec. 1992, respectively. She became a lecturer in Faculty of Automatic Control Engineering, Beijing University of Aeronautics and Astronautics of China in 1995. Her interest mainly includes the thin film optics and the semiconductor material.